

Article

# Evaporative Cooling Options for Building Air-Conditioning: A Comprehensive Study for Climatic Conditions of Multan (Pakistan)

Shazia Noor <sup>1,2</sup>, Hadeed Ashraf <sup>1</sup>, Muhammad Sultan <sup>1,\*</sup>  and Zahid Mahmood Khan <sup>1</sup>

<sup>1</sup> Department of Agricultural Engineering, Bahauddin Zakariya University, Multan 60800, Pakistan; shazianoor@bzu.edu.pk (S.N.); hadeedashraf15@gmail.com (H.A.); zahidmk@bzu.edu.pk (Z.M.K.)

<sup>2</sup> Department of Mechanical Engineering, Bahauddin Zakariya University, Multan 60800, Pakistan

\* Correspondence: muhammadsultan@bzu.edu.pk; Tel.: +92-333-610-8888

Received: 18 May 2020; Accepted: 8 June 2020; Published: 12 June 2020



**Abstract:** This study provides comprehensive details of evaporative cooling options for building air-conditioning (AC) in Multan (Pakistan). Standalone evaporative cooling and standalone vapor compression AC (VCAC) systems are commonly used in Pakistan. Therefore, seven AC system configurations comprising of direct evaporative cooling (DEC), indirect evaporative cooling (IEC), VCAC, and their possible combinations, are explored for the climatic conditions of Multan. The study aims to explore the optimum AC system configuration for the building AC from the viewpoints of cooling capacity, system performance, energy consumption, and CO<sub>2</sub> emissions. A simulation model was designed in DesignBuilder and simulated using EnergyPlus in order to optimize the applicability of the proposed systems. The standalone VCAC and hybrid IEC-VCAC & IEC-DEC-VCAC system configurations could achieve the desired human thermal comfort. The standalone DEC resulted in a maximum COP of 4.5, whereas, it was 2.1 in case of the hybrid IEC-DEC-VCAC system. The hybrid IEC-DEC-VCAC system achieved maximum temperature gradient (21 °C) and relatively less CO<sub>2</sub> emissions as compared to standalone VCAC. In addition, it provided maximum cooling capacity (184 kW for work input of 100 kW), which is 85% higher than the standalone DEC system. Furthermore, it achieved neutral to slightly cool human thermal comfort i.e., 0 to −1 predicted mean vote and 30% of predicted percentage dissatisfied. Thus, the study concludes the hybrid IEC-DEC-VCAC as an optimum configuration for building AC in Multan.

**Keywords:** Evaporative cooling systems; vapor compression air-conditioning; building air-conditioning; human thermal comfort; predicted mean vote (PMV); Pakistan

## 1. Introduction

Air-conditioning (AC) loads of buildings are increasing rapidly due to the increase in population, urbanization, and standards of living [1]. Although, many environment friendly AC systems are used nowadays that are free from HCFC/HFC refrigerants. However, there are many environmentally harmful systems that are still under practice to control/regulate temperature and humidity. Thus, increasing AC use is somehow responsible for global warming and CO<sub>2</sub> emissions around the globe [2]. Alternatively, heat-driven adsorption/absorption-based environment friendly AC systems are also in practical use [3,4]. In 2017, worldwide global electricity consumption in the residential sector was around 496,583 and 398,729 ktoe in commercial and public sector buildings, respectively [5]. Heating, ventilation and air-conditioning (HVAC) of buildings consume a huge amount of total building electricity, which is also responsible for the increase in CO<sub>2</sub> emissions [6,7]. Therefore, environment friendly HVAC systems are principally needed worldwide. Evaporative cooling systems

could provide low-cost and environment friendly alternative options for building AC load management. In some studies, the evaporative cooling systems are coupled with a conventional vapor compression air-conditioning (VCAC) system to achieve the desired levels of AC [8–12].

Evaporative cooling is a renowned and vintage cooling concept by which cooling is produced due to water-vapor evaporation into the process air. These systems are usually classified as direct (DEC), indirect (IEC), Maisotsenko-cycle i.e., M-cycle (MEC) evaporative cooling systems [2]. Standalone evaporative cooling systems usually achieve smaller temperature flux followed by lower cooling capacity as compared to VCAC systems, therefore, hybrid systems have also been explored in the literature [9]. In addition, several experimental and theoretical researches have been conducted for standalone and multistage evaporative cooling systems to achieve the required conditions of temperature and humidity. These include (but not limited to) IEC-DEC [13–15], DEC-IEC [16], VCAC-IEC [17], IEC-VCAC [18,19], DEC-VCAC [20–22], and IEC-DEC-VCAC [23].

A combined parallel-regenerative cooler was comparatively studied along with bi-stage counter flow and parallel flow indirect evaporative coolers [24]. Wet-bulb effectiveness (WBE) of the parallel-regenerative cooler was highest (i.e., 1.31) among the other configurations. An IEC system was coupled with VCAC, which drops 75% cooling load [25]. According to an experimental investigation [26], WBE of 1.11 is achieved in case of IEC-DEC system. In addition, power consumption dropped up to 60% when compared to VCAC system [26]. A numerical study for Mediterranean region employed a passive DEC system for the AC load management of an office buildings. The DEC resulted in being an effective cooling system in Eastern Mediterranean and southern Spain [27]. A spatiotemporal analysis of cooling potential of evaporative coolers and direct ventilation cooling techniques was performed in Iberia. Cooling thermal load savings in direct ventilation and evaporative cooling were 27% and 40%, respectively [28]. Lost heat in exhaust air was recovered by utilizing an evaporative cooling system in ventilation. Temperature gradients of 2.2 °C and 7.5 °C were observed at outside air temperatures of 24.4 °C and 35.7 °C, respectively. It shows that evaporative cooling efficiency is dependent on ambient air temperature [29]. Draught evaporative cooling was applied to official and public buildings. Dry bulb (DBT) minus wet-bulb (WBT) temperature index (DBT-WBT) was estimated for United States of America [30], which also justifies the dependence of the ambient air temperature.

Nowadays, many heat-driven AC systems such as adsorption/absorption systems are used which not only use environment friendly refrigerants but also use renewable energy sources. Therefore, these systems can also help to provide an alternative environment friendly AC system. Consequently, integration of desiccant units into evaporative coolers has been extensively studied in the literature to provide a sustainable solution [31–33]. Cooling capacity of a liquid desiccant system was enhanced by 41% when coupled with a dew-point IEC system [34]. Another evaporative cooling-assisted liquid desiccant system resulted in 12% lesser primary energy consumption for building cooling as compared to VCAC [35]. In addition, an evaporative cooling-based liquid desiccant system was experimentally investigated. A temperature gradient of 5.5 °C was found in the supply air [36]. Human thermal comfort for buildings was evaluated using evaporative cooling-based liquid desiccant AC system [37]. Predicted mean vote (PMV) method was used to determine the overall thermal comfort using TRNSYS simulation. The PMV was within the acceptable range of Standard 55 provided by American Society of Heating, Refrigerating and Air-Conditioning Engineers (ASHRAE). Similarly, solid desiccant system assisted by dewpoint evaporative cooler resulted in a 65% more efficient system than standalone desiccant AC (DAC) system [38]. Apart from building AC, the desiccant [39,40] and evaporative cooling systems have been investigated for various applications including agricultural product storage [41], greenhouse air-conditioning, and livestock air-conditioning etc. [41–46].

According to the above discussion, a thumb rule for evaporative cooling dictates “The hotter, the better”. Thereby, locally developed low-cost evaporative coolers are extensively used in Pakistan due to its typical summer conditions [47,48]. The Köppen–Geiger climate classification map for Pakistan is provided in Figure 1, which highlights considerable variation of climatic conditions across the country.

Buildings in Pakistan are generally built with brick wall with low to moderate insulation without any AC load calculation. The VCAC systems are usually preferred in commercial buildings, however, it is not financially feasible at least for low-income residents [21,49]. Therefore, multistage and/or hybrid types of evaporative coolers could be an eye-catching solution for providing desired conditions throughout year. Consequently, seven kinds of evaporative cooling configurations (DEC, IEC, VCAC, IEC-DEC, DEC-VCAC, IEC-VCAC, and IEC-DEC-VCAC) are explored in this study for climatic conditions of Multan (Pakistan). The effectiveness of evaporative cooling systems is determined from the lab-scale experimental apparatus, which are used as design values for DesignBuilder simulation. Building AC load of Agricultural Engineering Department of Bahauddin Zakariya University and associated human thermal comfort were estimated in EnergyPlus. Cooling capacity, coefficient of performance (COP) and reduction in CO<sub>2</sub> emissions by the systems were investigated and compared accordingly.

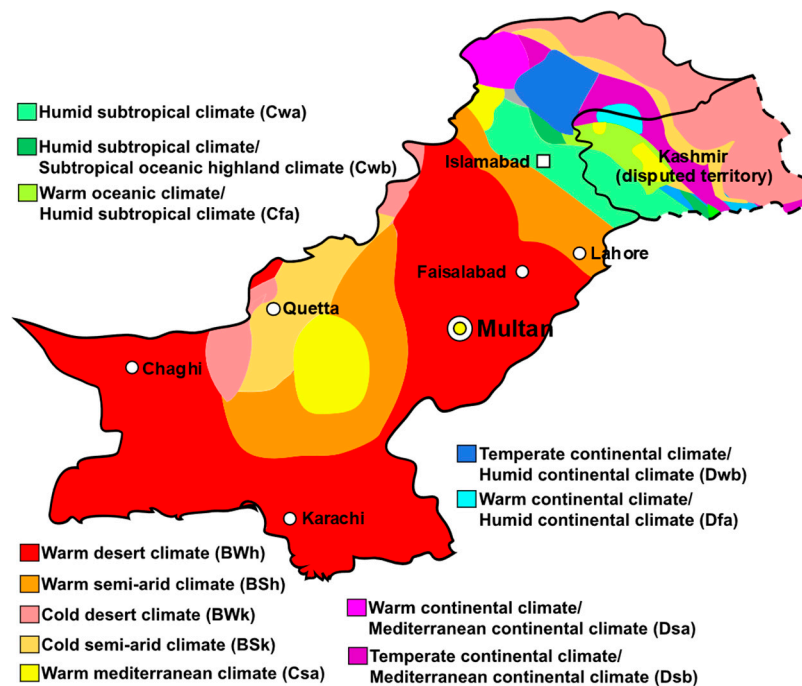


Figure 1. Köppen–Geiger climate classification map of Pakistan, reproduced from [47].

## 2. Proposed Evaporative Cooling Systems' Configuration

As the study area lies in a warm desert (hot and dry) climate (BWh) class of Köppen climate classification system [47], therefore, the EC systems are usually operated in the region except for monsoon (rainy) season. However, the potentials of multistage EC and hybrid systems are not explored as far as the local market of Pakistan is concerned. Therefore, this study investigates seven combinations of EC and VCAC systems, which are named as: (a) DEC, (b) IEC, (c) VCAC, (d) IEC-DEC, (e) DEC-VCAC, (f) IEC-VCAC, and (g) IEC-DEC-VCAC. Schematic illustrations and the corresponding psychrometric behavior are provided in Figure 2a–g, respectively. The key information for each proposed system is provided as follows:

- DEC system (Figure 2a): It cools process air isenthalpically (process 1–2). The DEC system can cool the process air up to wet-bulb temperature of the ambient air.
- IEC system (Figure 2b): The working air (process 1–3) is cooled isenthalpically like DEC, and the cooling affect is transferred to product air by heat transfer between wet and dry channels. The fact sensibly cools the product air (process 1–2) up to wet-bulb temperature.
- VCAC system (Figure 2c): It is the conventional compressor-based vapor compression air conditioning unit that cools the process air below the dew point. The required conditions are obtained by mixing/reheating the product air (process 1–2, dotted line).

- IEC-DEC (Figure 2d): It is a double stage EC unit that cools the air by indirect (process 1–2) followed by direct (process 2–3) EC concepts.
- DEC-VCAC (Figure 2e): It is a hybrid system composed of DEC (process 1–2) and VCAC (process 2–3) units.
- IEC-VCAC (Figure 2f): It is a hybrid system composed of IEC (process 1–2) and VCAC (process 2–3) units.
- IEC-DEC-VCAC (Figure 2g): It is also a hybrid system that is composed of IEC (process 1–2), IEC (process 2–3) and VCAC (process 3–4) units.

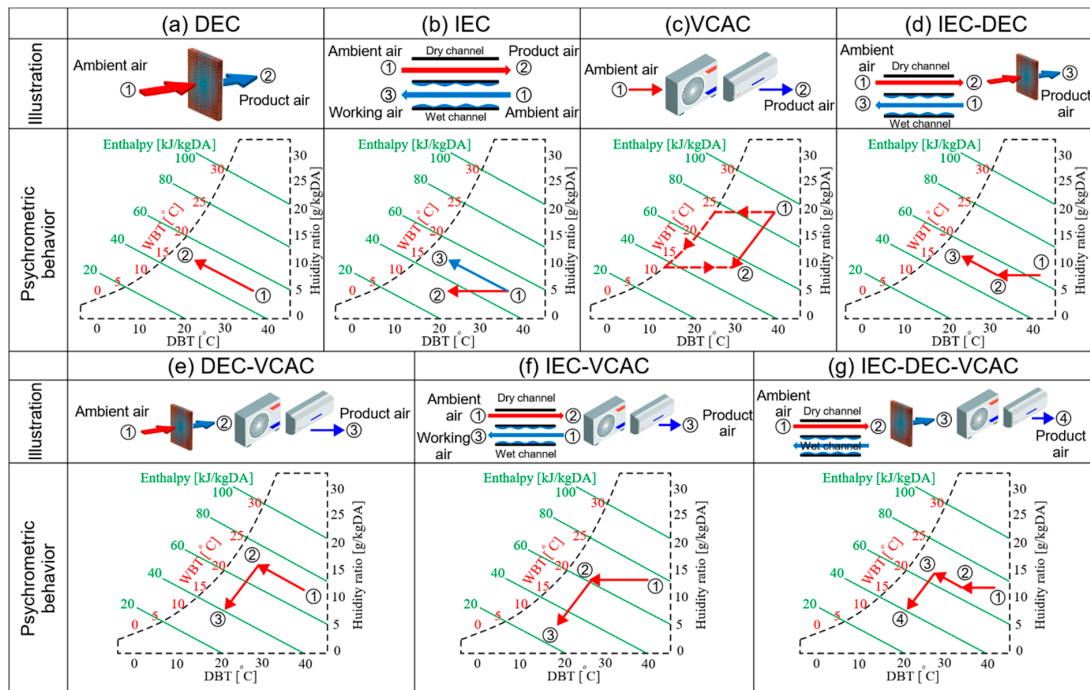


**Figure 2.** Schematic illustrations and the corresponding psychrometric behavior for seven proposed configurations of EC and VCAC systems: (a) DEC, (b) IEC, (c) VCAC, (d) IEC-DEC, (e) DEC-VCAC, (f) IEC-VCAC, and (g) IEC-DEC-VCAC.

### 3. Materials and Methods

#### 3.1. Building Energy Simulation

##### 3.1.1. Building Layout

The present study focuses on air-conditioning requirements for the building of the Agricultural Engineering Department of Bahauddin Zakariya University, Multan, Pakistan. The primary layout of the building is shown in Figure 3, which occupies a floor of 3251.7 m<sup>2</sup> area and volume of 15,669.0 m<sup>3</sup>. The details of inputs parameters used for simulation are provided in Table 1 and consist of building geometrical information (height, wall/ roof construction material, glazing/window construction material, and overall heat transfer coefficient), thermal gains, energy efficiency setpoints, and zone-wise AC operation schedule.

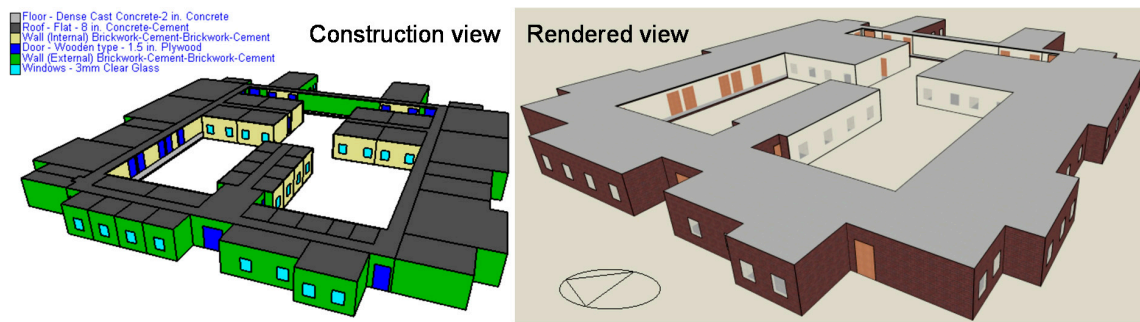


**Figure 3.** 3-D model for the studied building of the Agricultural Engineering Department of Bahauddin Zakariya University, Multan, Pakistan: (a) constructed view, and (b) rendered view.

**Table 1.** Simulation inputs and building construction characteristics.

Construction Type	Properties	Values
Layer 1 (outer wall)	Brickwork outer	0.1016 m
Layer 2 (outer wall)	Cement/plaster/mortar—cement	0.0127 m
Layer 3 (outer wall)	Brickwork inner	0.1016 m
Layer 4 (outer wall)	Cement/plaster/mortar—cement	0.0127 m
Medium weight flat roof Layer 1	8 in. concrete	0.2032 m
Medium weight flat roof Layer 2	Cement/plaster/mortar—cement	0.0127 m
Floor (Layer 1)	Cast concrete (dense)	0.127 m
Floor (Layer 2)	2 in. concrete	0.0508 m
Doors	Lightweight plywood	0.0381 m
Glazing/ window	Generic clear	0.003 m
Fixed height/width	Height	1.83 m
-	Width	1.52 m
Frame type/width	Aluminum	0.04 m
	Total building area	3251.74 m <sup>2</sup>
	Total conditioned area	847.5 m <sup>2</sup>
Density Inputs		
Lighting power density	Normalized (varies zone to zone)	2.5 W m <sup>-2</sup>
-	Radiant fraction	0.72
-	Visible fraction	0.18
Occupancy	Density (varies zone to zone)	0.295/conditioned area
Workday schedule	On at	08:00 am
-	Off at	04:00 pm
Clothing ( <i>Shalwar, Kameez</i> ) [50,51]	Winter	1.145 clo
(1 clo = 0.155 m <sup>2</sup> °C W <sup>-1</sup> )	Summer	0.775 clo
Air Handling Unit (AHU)		
Fan	Total efficiency	75%
Fan type	Constant air volume (CAV)	
AHU type	Central air-conditioning system	
	Motor efficiency	85%
	Fan pressure	600 Pa
	COP of VCAC	3
	Thermostat and humidistat setpoint	24 °C and 60%
Direct research special	Design wet-bulb effectiveness (WBE)	0.90
Indirect research special	Design WBE	0.605

### 3.1.2. Energy Simulation

The DesignBuilder [52] coupled with EnergyPlus [53] is extensively considered as effective and authoritative software for building simulation as compared to eQuest, Elements, and Sketchup [19,54–76]. Therefore, preliminary layout, thermal properties, construction materials,

overall thermal coefficient, building symmetry, direction, and all other physical properties for the studied building were designed in DesignBuilder and simulated using EnergyPlus. The proposed seven combinations for AC units (Figure 2) were designed in DesignBuilder using HVAC module in generic loop air handling unit (AHU). Hourly weather data of Multan (Pakistan) are used for the simulation, which was obtained from TRNSYS repository, provided by World Meteorological Organization (WMO) [77], cross checked using station weather data from Meteonorm. A complete fresh air circulation in AHU was selected. The modules of Direct Research Special and Indirect Research Special were selected in DesignBuilder for DEC and IEC analyses with design WBE of 0.90 and 0.605, respectively (Table 1). A direct expansion (DX) cooling coil was used in the case of the VCAC system. Thereby, combinations of single stage, multistage, and hybrid AC systems were successively arranged inside the AHU.

The corridors of the studied building are excluded from simulation as they are exposed to atmosphere. The washrooms area is also excluded from simulation as local design. The operation schedule for seven AC system configuration was selected from 8 am to 4 pm, which are typical office hours in the building.

### 3.2. Energy Estimations

Wet-bulb effectiveness (WBE) can be calculated by the ratio of temperature differences as given by [2]:

$$\varepsilon_{wb} = \frac{T_{OA,DBT} - T_{SA,DBT}}{T_{OA,DBT} - T_{OA,WBT}} \quad (1)$$

where,  $\varepsilon_{wb}$  is WBE (-) and  $T$  is temperature ( $^{\circ}\text{C}$ ). The subscripts  $OA$  and  $SA$  represent outside air and supply air, respectively. The subscripts  $DBT$  and  $WBT$  represent dry bulb and wet-bulb temperatures, respectively. Cooling capacity ( $Q$ ) was determined using Equation (2) as given by [78]:

$$Q = mC_p(\Delta T) \quad (2)$$

where,  $Q$  denotes the cooling capacity (kW),  $m$  denotes air mass flow rate of  $\sim 14 \text{ kg s}^{-1}$ ,  $C_p$  represents specific heat capacity of air ( $1.005 \text{ kJ kg}^{-1} \text{ K}^{-1}$ ), and  $\Delta T$  is the difference between outside and supply air temperatures ( $^{\circ}\text{C}$ ). Coefficient of performance (COP) was defined as the ratio of the cooling effect produced to the work input (prime movers, fans), represented by Equation (3):

$$\text{COP} = \frac{Q}{W} \quad (3)$$

Equation (2) was also used for VCAC with an assumption of no latent heat transfer. However, considering latent heat transfer, Equations (4)–(7) can be used as given by [53]:

$$m = \rho_{air}u \quad (4)$$

$$Q_{net} = m(h_{out} - h_{in}) \quad (5)$$

$$Q_{sensible} = m(h_{out} - h_{in})X_{min} \quad (6)$$

$$Q_{latent} = Q_{net} - Q_{sensible} \quad (7)$$

where,  $\rho_{air}$  represents density of air ( $\text{kg m}^{-3}$ ),  $u$  denotes the user-set volumetric flow of air ( $\text{m}^3 \text{ s}^{-1}$ ),  $h_{out}$  is total enthalpy of the air at supply side (J/kg),  $h_{in}$  is total enthalpy of the air at inlet side (J/kg),  $X_{min}$  is minimum of inlet and outlet air humidity ratios (kg/kg),  $Q_{net}$  is the total cooling capacity (W),  $Q_{sensible}$  is the total sensible energy transfer (W), and  $Q_{latent}$  is the total latent energy transfer (W).

### 3.2.1. Cooling Loads

Cooling loads faced by the AC system were classified into transmission, infiltration, internal, and equipment loads. Transmission loads are mainly generated from heat transfer from walls, roof, basement, and windows. Infiltration loads include air change through the opening of doors, clearance beneath the doors, cracks, and crawl spaces. Internal loads include heat generated from the human body, lighting, appliances, and solar heat gain from windows through conduction. Heat generated from the human body depends on the level of activity of the body in terms of metabolic rate. Typically, a seated office worker generates  $65 \text{ W m}^{-2}$  [50] heat varied by body surface area as given by Equation (8) [79]:

$$Area_{human\ body} = 0.202mass^{0.425}height^{0.725} \quad (8)$$

Thermal comfort of a human body mainly depends on operative temperature (approximately equal to the average of dry bulb temperature of air and surrounding surfaces' temperature), relative humidity and velocity of air. As per well-known heat and mass transfer guidelines by Cengel Y. [80], lower and upper acceptable limits of operative temperature for typical Pakistani *shalwar-kameez* clothing [50,51] are  $18^\circ\text{C}$  and  $23^\circ\text{C}$  (for winter: 1.145 clo) and  $21^\circ\text{C}$  and  $25^\circ\text{C}$  (for summer: 0.775 clo), respectively, at 50% relative humidity and air flow of  $0.15 \text{ m s}^{-1}$  [80]. The heat gains through human body ( $Q_{hb}$ ), exterior surfaces ( $Q_{ext}$ ), sol-air temperature ( $T_{s-a}$ ), walls ( $Q_{wall}$ ), fan motors ( $Q_m$ ), floor ( $Q_{sp}$ ), windows ( $Q_{glazing}$ ), air change per hour (ACH), sensible infiltration ( $Q_{s,i}$ ), and latent infiltration ( $Q_{l,i}$ ) were calculated by Equations (9)–(18), respectively [80]. For details, please refer to the cited literature [78].

$$Q_{hb} = (Q_{sens} + Q_{lat})_{skin} + (Q_{sens} + Q_{lat})_{lungs} \quad (9)$$

$$Q_{ext} = h_o A_s (T_a - T_s) + \alpha_{solar} A_s q_{solar} - E A_s \varphi (T_a^4 - T_{sur}^4) \quad (10)$$

$$T_{s-a} = T_a + \frac{\alpha_{solar} q_{solar}}{h_o} - \frac{E \varphi (T_a^4 - T_{sur}^4)}{h_o} \quad (11)$$

$$Q_{wall} = U_{wall} A_s (T_{s-a} - T_{in}) \quad (12)$$

$$Q_m = \frac{P_r L_f U_f}{\eta_m} \quad (13)$$

$$Q_{sp} = U_{floor} P_{floor} (T_{in} - T_{out}) \quad (14)$$

$$Q_{glazing} = Q_c + Q_e + Q_f = U_g A_g (T_{in} - T_{out}) \quad (15)$$

$$ACH = \frac{m_{in}}{V} \quad (16)$$

$$Q_{s,i} = \rho_{air} C_p ACH V (T_{in} - T_{out}) \quad (17)$$

$$Q_{l,i} = \rho_{air} h_{fg} ACH V (X_{in} - X_{out}) \quad (18)$$

where,  $Q_{hb}$  denotes total heat generated from human body (W);  $Q_{sens}$  represents sensible heat gain from the skin and lungs;  $Q_{lat}$  represents latent heat from the body (sweating, moist breath);  $h_o$  represents heat transfer coefficient ( $\text{W m}^{-2} \text{ }^\circ\text{C}$ );  $A_s$  represents surface area of the wall ( $\text{m}^2$ );  $T_a$  stands for ambient air temperature ( $^\circ\text{C}$ );  $T_s$  represents surface temperature ( $^\circ\text{C}$ );  $\alpha_{solar}$  represents solar absorptivity constant [81];  $q_{solar}$  represents incident solar radiation ( $\text{W m}^{-2}$ );  $E$  represents surface emissivity [50];  $\varphi$  represents solar incident angle relative to the latitude;  $T_{sur}$  represents mean temperature of surrounding surfaces ( $^\circ\text{C}$ );  $T_{s-a}$  denotes sol-air temperature ( $^\circ\text{C}$ );  $U_{wall}$  represents wall's overall heat transfer coefficient ( $\text{W m}^{-1} \text{ }^\circ\text{C}^{-1}$ );  $T_{in}$  and  $T_{out}$  represent inside and outside air temperatures, respectively;  $Q_m$  represents heat gain from motor (W);  $P_r$  represents power of the motor (W);  $L_f$  represents load factor;  $U_f$  represents utilization factor and  $\eta_m$  denotes efficiency of the motor;  $Q_{sp}$  represents total heat loss from the floor (W);  $U_{floor}$  represents overall heat transfer coefficient for the floor ( $\text{W m}^{-1} \text{ }^\circ\text{C}^{-1}$ );  $P_{floor}$

represents floor perimeter (m);  $Q_{glazing}$  represents total heat transfer through the windows;  $Q_c$ ,  $Q_e$ , and  $Q_f$  represent heat transfer through center, edge and frame of the windows, respectively;  $U_g$  represents overall heat transfer coefficient of the window;  $A_g$  denotes surface area of the window;  $ACH$  represents air change/hour;  $m_{in}$  represents air infiltration inflow rate ( $\text{m}^3 \text{h}^{-1}$ );  $V$  represents building volume ( $\text{m}^3$ );  $Q_{s,i}$  and  $Q_{l,i}$  represent sensible and latent heat transfer due to infiltration, respectively;  $h_{fg}$  represents latent heat of evaporation ( $\text{kJ kg}^{-1}$ ); and  $X_{in}$  &  $X_{out}$  represent inside and outside air humidity ratios ( $\text{g/g}$ ), respectively.

### 3.2.2. Thermal Comfort Indices

Thermal comfort can be quantified using predicted mean vote ( $PMV$ ) and predicted percentage of dissatisfaction ( $PPD$ ) as per Fanger's model and ISO standard 7730 [82]. Thermal comfort is a structure of various factors including temperature, relative humidity, velocity of air, rate of human body metabolism (directly linked to performance activity), and clothing insulation. It is important to note that  $PMV$  is only an average of thermal comfort sensation for a group of persons, so, individual thermal comfort sensation can vary from this average value. To counter this effect,  $PPD$  (as a function of  $\pm 2 PMV$ ) is introduced. The  $PMV$  and  $PPD$  was calculated using Equations (19)–(22) [82] and Equation (23) [82]:

$$PMV = [0.303 e^{(-0.036Met)} + 0.028](Met - Q_{work}) - 3.05[5.73 - 0.007(Met - Q_{work}) - P_a] - 0.42[(Met - Q_{work}) - 58.15] - 0.0173 Met(5.87 - P_a) - 0.0014 Met(34 - T_{air}) - 3.96 e^{-8} r_{cb}[(T_{cloth} + 273)^4 - (MRT + 273)^4] - r_{cb} h_{conv}(T_{cloth} - T_{air}) \quad (19)$$

$$T_{cloth} = 35.7 - 0.0275(Met - Q_{work}) - R_c\{ (Met - Q_{work}) - 3.05[5.73 - 0.007(Met - Q_{work}) - P_a] - 0.42[(Met - Q_{work}) - 58.15] - 0.0173 Met(5.87 - P_a) - 0.0014 Met(34 - T_{air}) \} \quad (20)$$

$$h_{conv} = \begin{cases} 2.38(T_{cloth} - T_{air})^{0.25} & \text{for } 2.38(T_{cloth} - T_{air})^{0.25} > 12.1 \sqrt{u_{air}} \\ 12.1 \sqrt{u_{air}} & \text{for } 2.38(T_{cloth} - T_{air})^{0.25} < 12.1 \sqrt{u_{air}} \end{cases} \quad (21)$$

$$r_{cb} = \begin{cases} 1.0 + 0.2 Cloth_{insul} & \text{for } Cloth_{insul} < 0.5 clo \\ 1.05 + 0.1 Cloth_{insul} & \text{for } Cloth_{insul} > 0.5 clo \end{cases} \quad (22)$$

$$PPD = 100 - 95 e^{(-0.03353PMV^4 - 0.2179PMV^2)} \quad (23)$$

where,  $Met$  represents metabolic rate of the body per unit area ( $\text{W m}^{-2}$ ),  $Q_{work}$  represents heat loss from working human body ( $\text{W m}^{-2}$ ),  $P_a$  vapor pressure of ambient air,  $T_{air}$  represents temperature of the conditioned space ( $^{\circ}\text{C}$ ),  $r_{cb}$  represents ratio of clothed to naked body,  $T_{cloth}$  represents temperature of the clothes ( $^{\circ}\text{C}$ ),  $MRT$  represents mean radiant temperature ( $^{\circ}\text{C}$ ),  $h_{conv}$  represents convective heat transfer coefficient of the conditioned space ( $\text{W m}^{-2} \text{ } ^{\circ}\text{C}^{-1}$ ),  $R_c$  represents thermal resistance of clothes ( $\text{m}^2 \text{ } ^{\circ}\text{C W}^{-1}$ ),  $u_{air}$  represents velocity of air flow ( $\text{m s}^{-1}$ ), and  $Cloth_{insul}$  represents insulation of clothes (clo).

## 4. Results and Discussion

Figure 4 shows the numerical values of WBE achieved by DEC and IEC systems for climatic conditions of Multan (Pakistan) [83]. The effectiveness results presented in Figure 4 cover the typical summer months (i.e., May to August) under Multan conditions. These results are based on the lab-scale DEC/IEC experimental apparatus from the authors' previous work [83]. The details of experiments are not provided in this study for simplicity and ease of simulation. Consequently, WBE numerical values of 0.90 and 0.605 are used as design values in the simulation models for DEC and IEC systems,

respectively (Table 1). Consequently, a simulation model was designed in DesignBuilder and simulated using EnergyPlus to optimize the applicability of the proposed seven systems (Figure 2) for the studied building in Multan (Pakistan). The details of study area, AC load, and simulation are provided in Section 3. Accordingly, the results are presented in Figure 5a–b for a monthly basis, which shows the ambient and product air conditions for all of the seven AC configurations for temperature, relative humidity, humidity ratio, and enthalpy, respectively.

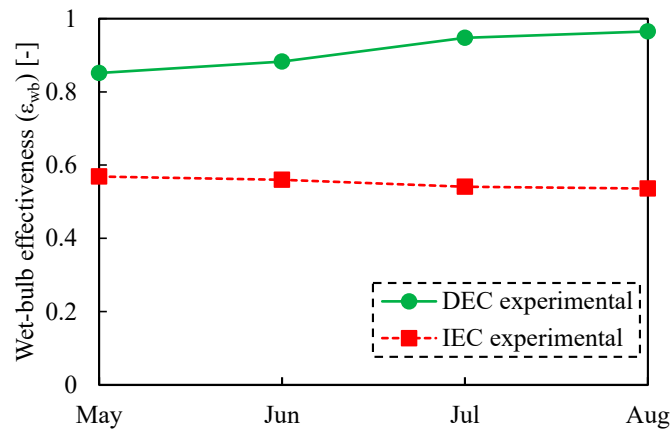


Figure 4. Wet-bulb effectiveness determined from lab-scale DEC and IEC experimental apparatus for summer climatic conditions of Multan [83].

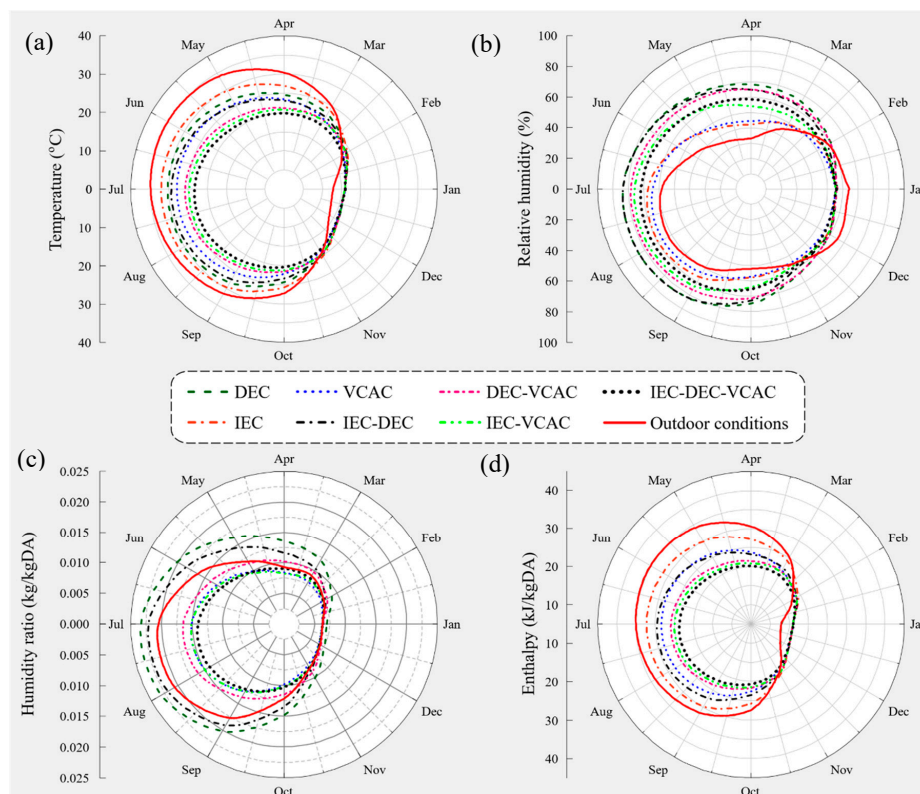
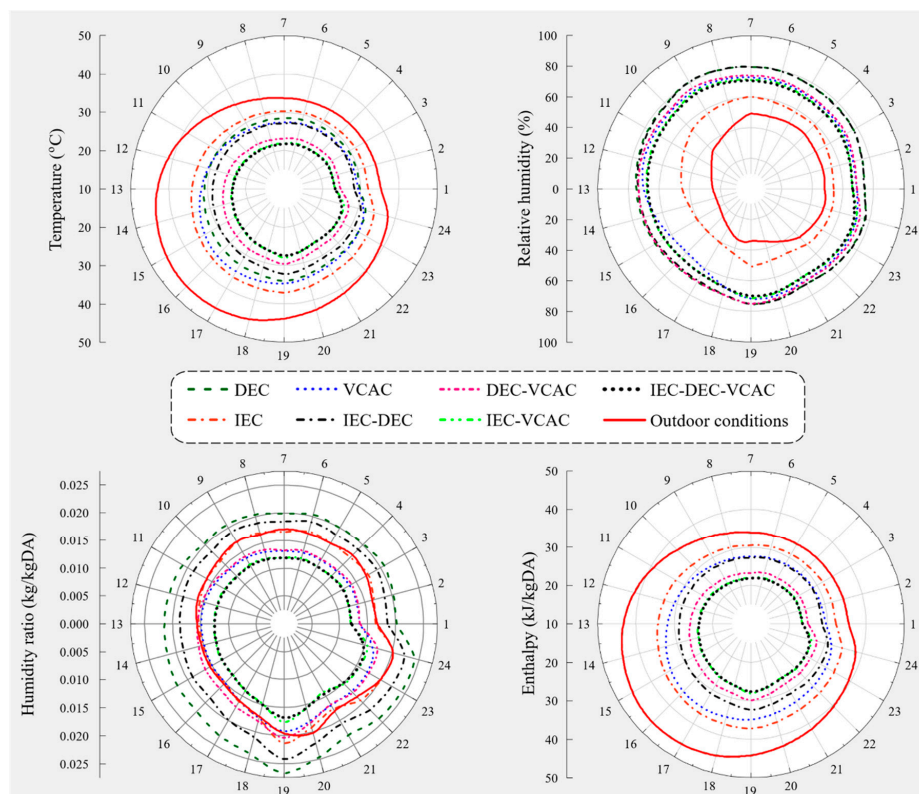


Figure 5. Performance evaluation on monthly basis for the proposed seven AC system configurations using annual climatic data.

The IEC-DEC-VCAC system provided a temperature gradient of 13 °C (maximum) in May, whereas the IEC system was only able to achieve 4 °C (Figure 5a). It is important to mention that the temperature gradient is defined as the difference between ambient and product air temperatures.

The studied hybrid system options (i.e., DEC-VCAC, IEC-VCAC and IEC-DEC-VCAC) performed relatively better as compared to all standalone system options. The standalone VCAC system resulted in a temperature gradient of 7 °C in May, which also produces almost uniform performance irrespective of ambient conditions round the clock throughout the month. Maximum temperature gradient for all configurations was found mostly in May and June months, whereas it was negative in winter months. The DEC system provided a relative humidity difference of 36% (maximum) in May (Figure 5b). The DEC system provided a humidity ratio of 0.000023 kg kg<sup>-1</sup> in July (Figure 5c). The DEC system provided the highest enthalpy of 35.13 kJ kg<sup>-1</sup> in June (Figure 5d).

In support to the above discussion, an insight of hourly performance variation is presented in Figure 6 for all configurations accordingly. The presented results are depicted for 19 June conditions as a hypothetical representative of a summer day. The findings of these hourly results are not much different, as reported above. Among the studied systems, the IEC-DEC-VCAC system resulted in a maximum temperature gradient i.e., 21 °C (at 3 pm) followed by IEC-VCAC i.e., 20.7 °C (at 3 pm), whereas the IEC system provided the lowest temperature gradient of just 9.8 °C (at 3 pm). From midnight to three past blazing noon, standalone EC systems resulted in a temperature gradient which depended on ambient air. It solidifies the statement that performance of standalone EC systems is dependent on ambient air conditions. In contrast, standalone VCAC and hybrid EC systems were only impacted by varying load. The hybrid EC systems easily meet the required conditions at higher power consumption.



**Figure 6.** Performance evaluation on hourly basis for the proposed seven AC system configurations using climatic data of 19 June.

One-day-averaged product air conditions of the seven AC systems are presented in Figure 7. It is worth mentioning that the expanded psychrometric chart with radiation and convection dimensions used in Figure 7 is taken in raw form from a state-of-the-art study authored by Teitelbaum et al. [84]. The IEC-DEC-VCAC resulted in a neutral to slightly cool thermal comfort sensation as per ISO 7730 [82] requirements (with matching mean radiant temperature *MRT*) for a person doing light office work,

whereas the IEC-VCAC system resulted in neutral to slightly warm thermal comfort sensation due to varying MRT. The standalone VCAC resulted in a few shades of discomfort. The DEC showed maximum deviation from its mean radiant temperature.

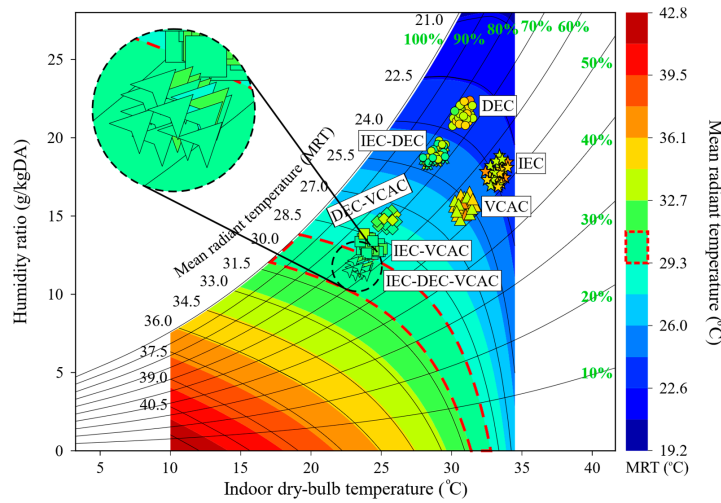


Figure 7. Profile of thermal comfort correlating with MRT for all the seven AC configurations.

From the PMV and PPD point of view, hourly annual thermal comfort sensation resulted from the seven AC configurations and is presented in Figure 8. All the proposed AC configurations achieved thermal comfort at some point or another throughout the whole year. However, on 19 June, all the hybrid EC systems (i.e., DEC-VCAC, IEC-VCAC and IEC-DEC-VCAC) achieved neutral to slightly cool thermal sensation with PPD variation of 30% to 40% (Figure 8).

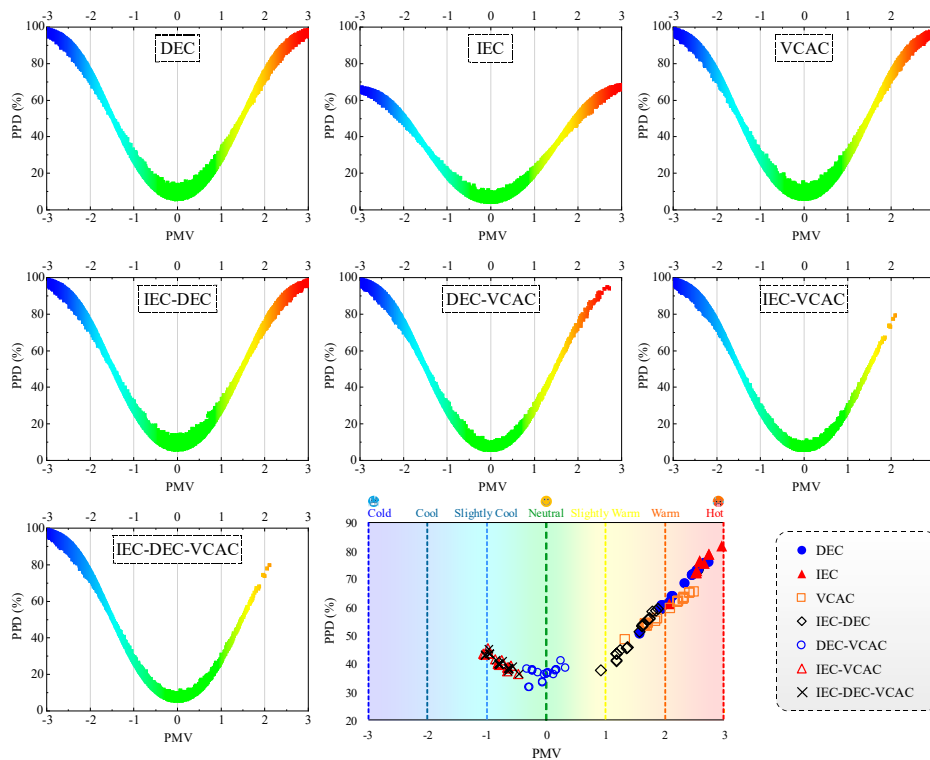


Figure 8. Annual variation of thermal comfort indices of the seven AC configurations.

Performance of the seven AC systems based on the temperature gradient specifically in summer months (May, June, July, August) is presented in Figure 9. The IEC-DEC-VCAC system provided a

temperature gradient of 10.9 °C (maximum) followed by 10.8 °C, 9.9 °C, 6.5 °C, 5.8 °C, 5.1 °C, and 3.2 °C (minimum) provided by IEC-VCAC, DEC-VCAC, IEC-DEC, VCAC, DEC, and IEC, respectively.

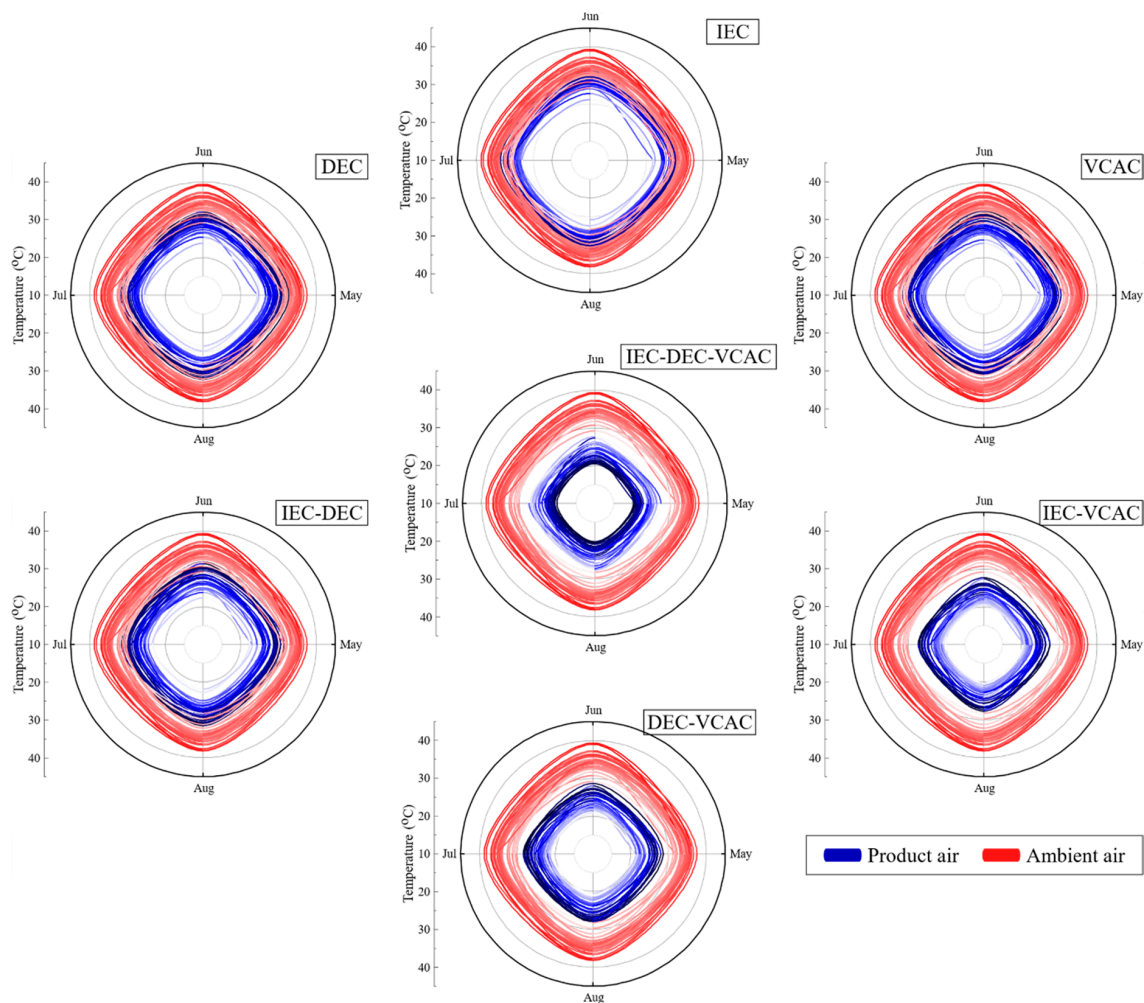


Figure 9. Profile of temperature gradient in typical summer months of Multan.

Performance of the seven AC configurations based on 1-day-averaged WBE for the climatic conditions of Multan (Pakistan) is presented in Figure 10. The IEC-DEC-VCAC system provided maximum WBE of 1.5 followed by IEC-VCAC i.e., 1.45, whereas, the standalone IEC system provided WBE of 0.5 (minimum). All the hybrid EC systems provided WBE of more than 1 due to pretreatment in EC stage and further compression at VCAC stage.

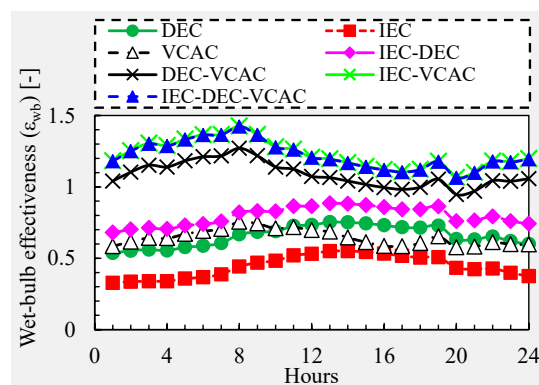
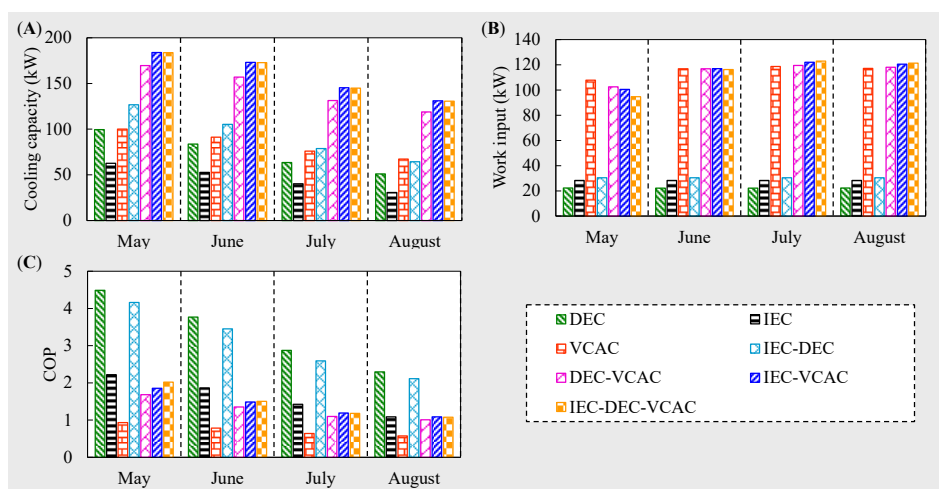


Figure 10. One-day-averaged variation of wet-bulb effectiveness of the seven AC configurations.

Variation in cooling capacity, work input and COP of the seven AC systems for summer months is presented in Figure 11a–c, respectively. The IEC-DEC-VCAC system provided the highest cooling capacity of 184 kW, followed by IEC-VCAC with 183.5 kW, whereas, the standalone IEC system provided the lowest cooling capacity of 63 kW (Figure 11a). The standalone EC systems provided the lowest work input of 20 to 30 kW compared to the VCAC system with 108 kW. It is important to note that IEC-DEC-VCAC provided relatively lower work input among the VCAC-based systems (Figure 11b). The standalone DEC system provided the highest COP of 4.5 followed by the IEC-DEC system with 4.2 due to relatively lower work input. It is also worth mentioning that the IEC-DEC-VCAC system provided a relatively higher COP of 2 among the VCAC-based systems (Figure 11c). VCAC-based AC systems resulted in low COP compared to the DEC and IEC-DEC systems due to higher work input at direct expansion stage (cooling coil). In addition, the details of annual electricity consumption (kWh) of the studied AC system configurations are provided in Figure S1 (Supplementary Materials).



**Figure 11.** Variation in (a) Cooling capacity, (b) work input, and (c) COP of the seven AC configurations in summer.

Figure 12 depicts the annual water consumption by the seven AC systems. The IEC-DEC system resulted in the highest water consumption of 1256 m<sup>3</sup> year<sup>-1</sup> due to multistage EC systems followed by 1245, 1045, 1035, 704, and 697 m<sup>3</sup> year<sup>-1</sup> water consumption by the IEC-DEC-VCAC, DEC, DEC-VCAC, IEC, and IEC-VCAC systems, respectively. The standalone VCAC system consumed no water for cooling due to usage of air-cooled coil. All the hybrid systems provided relatively lower water consumption compared to their respective standalone systems.

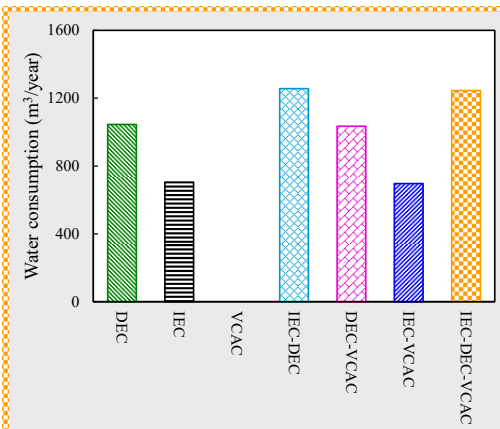


**Figure 12.** Annual end-use water consumption for cooling by the seven AC configurations.

Additionally, annual sensible and latent heat gains from different sources (i.e., surface conduction, windows, people, infiltration, and equipment and lights) into the building are presented in Figure 13. Surface conduction contributed the highest heat gain of 79.1% of the total heat gains. Heat gain from surface conduction is highest due to poor insulation of walls and roof during building construction in Pakistan. Based on the above discussions, it was concluded that the EC hybrid systems, especially the IEC-DEC-VCAC system provides a superior performance compared to other AC systems. Although COP of IEC-DEC-VCAC is lesser compared to other AC systems due to higher work input, this system provided the highest cooling capacity and WBE, and it can achieve the required conditions subject to a higher power consumption rate.

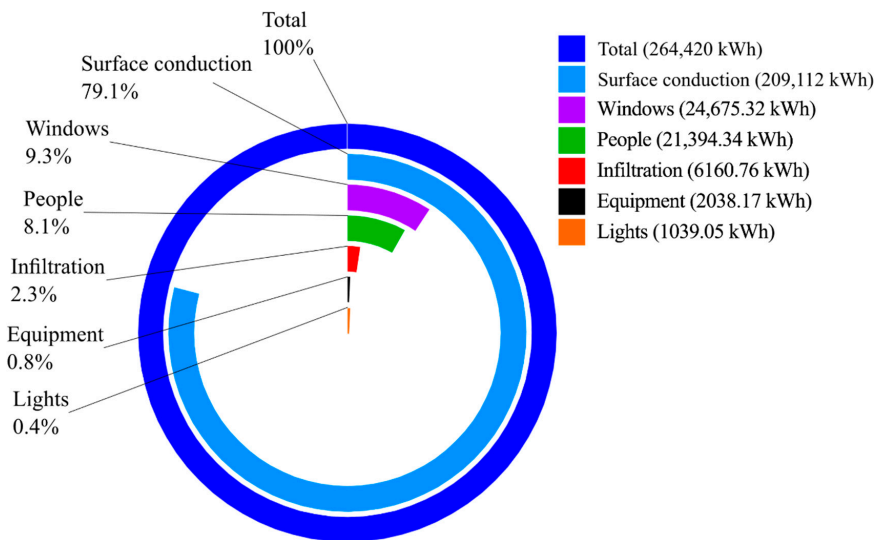


Figure 13. Annual energy nexus-sensible heat gains from different sources in the building.

Annual greenhouse gas (CO<sub>2</sub>) emissions from the seven AC configurations is presented in Figure 14. CO<sub>2</sub> emissions were obtained by multiplying the annual electricity consumption with the CO<sub>2</sub> emission equivalent of 0.505 kgCO<sub>2</sub> kWh<sup>-1</sup> [85]. The DEC system emitted a minimum CO<sub>2</sub> i.e., 332.8 kgCO<sub>2</sub> year<sup>-1</sup> due to the absence of a compressor followed by IEC, with 129.74 kgCO<sub>2</sub> year<sup>-1</sup>. Among the VCAC-based systems, standalone VCAC system emitted the highest CO<sub>2</sub> of 274,883 kgCO<sub>2</sub> year<sup>-1</sup>. Moreover, the IEC-DEC-VCAC system emitted relatively the lowest CO<sub>2</sub> of 241,134 kgCO<sub>2</sub> year<sup>-1</sup> among the VCAC hybrid systems.

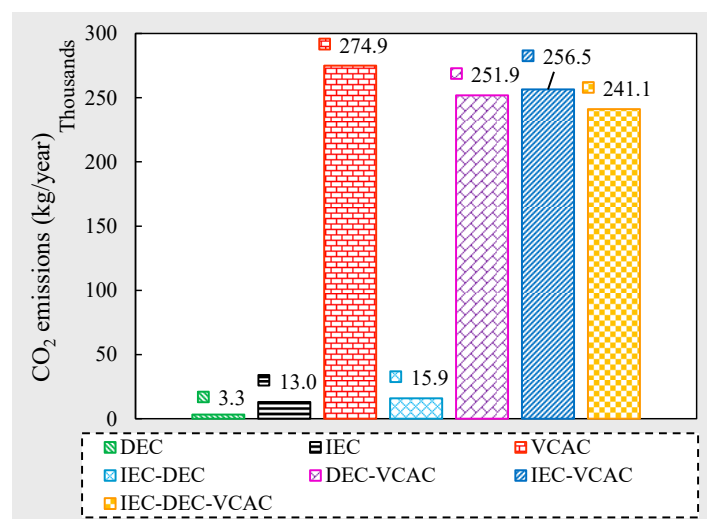


Figure 14. Annual CO<sub>2</sub> emissions of the proposed cooling systems in the building.

## 5. Conclusions

The present study aimed to explore the optimum AC system configuration comprised of direct evaporative cooling (DEC), indirect evaporative cooling (IEC), and vapor compression AC (VCAC) systems for the climatic conditions of Multan (Pakistan). The study area lies in a warm desert (hot and dry) climate (BWh) class of Köppen climate classification. In this regard, building AC load and human thermal comfort requirements for the Agricultural Engineering Department building of Bahauddin Zakariya University, Multan, Pakistan, have been investigated. Standalone evaporative cooling and standalone vapor compression AC (VCAC) systems are commonly used in Pakistan. Therefore, the study proposed seven AC system configurations named as: DEC, IEC, VCAC, IEC-DEC, DEC-VCAC, IEC-VCAC, and IEC-DEC-VCAC. The systems were designed in DesignBuilder and simulated using EnergyPlus.

The IEC-DEC-VCAC system provided a temperature gradient of 21 °C (maximum) subject to a higher power consumption, whereas, standalone EC systems failed to compete. All three hybrid systems achieved neutral to slightly cool *PMV* thermal comfort with 30 to 40% *PPD*. The IEC-DEC-VCAC system provided the highest WBE and cooling capacity of 1.4 and 184 kW, respectively. On the other hand, the IEC system provided the lowest WBE and cooling capacity of 0.50 and 63 kW, respectively. The DEC system yielded the highest COP of 4.5, whereas the IEC-DEC-VCAC system provided a low COP of ~2.0 due to higher work input. The IEC-DEC-VCAC emitted an average annual CO<sub>2</sub> of 241,134 kg of CO<sub>2</sub> per year. Among the seven AC configurations, the standalone VCAC system resulted in the highest annual CO<sub>2</sub> emissions i.e., 274,883 kg of CO<sub>2</sub> per year. The standalone VCAC and hybrid IEC-VCAC & IEC-DEC-VCAC system configurations could achieve the desired human thermal comfort for the study area. However, the study concludes the hybrid IEC-DEC-VCAC as an optimum configuration (among the studied options) for building AC in Multan due to its better performance in terms of temperature gradient, thermal comfort, and CO<sub>2</sub> emissions.

**Supplementary Materials:** The following are available online at <http://www.mdpi.com/1996-1073/13/12/3061/s1>, Figure S1: Annual electricity consumption (kWh) of different AC configurations.

**Author Contributions:** Conceptualization, S.N.; methodology, S.N. and H.A.; software, S.N. and H.A.; validation, H.A. and M.S.; formal analysis, S.N. and H.A.; investigation, S.N.; data curation, H.A.; writing—original draft preparation, S.N.; writing—review and editing, S.N., H.A. and M.S.; visualization, Z.M.K.; supervision, M.S. and Z.M.K.; project administration, M.S.; funding acquisition, M.S. All authors have read and agreed to the published version of the manuscript.

**Funding:** This research received no external funding.

**Acknowledgments:** All this work is part of the Ph.D. research of Shazia Noor (1st Author). This research work has been carried out in the Department of Agricultural Engineering, Bahauddin Zakariya University, Multan-Pakistan. This research was funded by Bahauddin Zakariya University, Multan-Pakistan under the Director Research/ORIC grant entitled “Development and performance evaluation of prototypes of direct and indirect evaporative cooling-based air conditioning systems” awarded to Principal Investigator Muhammad Sultan.

**Conflicts of Interest:** The authors declare no conflict of interest.

## Nomenclature

$\Delta T$	Difference between outside and supply air temperatures (°C)
AC	Air-conditioning
ACH	Air change per hour
$A_g$	Surface area of window (m <sup>2</sup> )
AHU	Air handling unit
$A_s$	Surface area of wall (m <sup>2</sup> )
ASHRAE	American Society of Heating, Refrigerating and Air-Conditioning Engineers
clo	Clothing insulation unit (1 clo 0.155 m <sup>2</sup> °C W <sup>-1</sup> )
$Cloth_{insul}$	Clothing insulation (clo)
COP	Coefficient of performance
$C_p$	Specific heat capacity of air (1.005 kJ kg <sup>-1</sup> K <sup>-1</sup> )

DAC	Desiccant air-conditioning system
DBT	Dry bulb temperature
DEC	Direct evaporative cooling system
DX	Direct expansion
$E$	Surface emissivity constant
EC	Evaporative cooling systems
$h_{conv}$	Convective heat transfer coefficient ( $W m^{-2} °C^{-1}$ )
$height$	Height of human body (m)
$h_{fg}$	Latent heat of evaporation ( $kJ kg^{-1}$ )
$h_{in}$	Total enthalpy of air at inlet side ( $J kg^{-1}$ )
$h_o$	Heat transfer coefficient ( $W m^{-2} °C$ )
$h_{out}$	Total enthalpy of air at supply side ( $J kg^{-1}$ )
HVAC	Heating, ventilation, and air-conditioning
IEC	Indirect evaporative cooling system
$L_f$	Load factor of motor
$m$	Mass flow rate ( $kg s^{-1}$ )
MEC	Maisotsenko-cycle based evaporative cooling
$Met$	Metabolic rate of body per area ( $W m^{-2}$ )
$m_{in}$	Air infiltration inflow rate ( $m^3 h^{-1}$ )
MRT	Mean radiant temperature ( $°C$ )
$P_a$	Vapor pressure of air (Pa)
$P_{floor}$	Floor perimeter (m)
PMV	Predicted mean vote
PPD	Predicted percentage of dissatisfaction (%)
$P_r$	Power of motor (W)
$Q$	Cooling capacity (kW)
$Q_c$	Heat transfer through center of glazing (W)
$Q_e$	Heat transfer through edge of glazing (W)
$Q_{ext}$	Heat gains through exterior surfaces (W)
$Q_f$	Heat transfer through frame of glazing (W)
$Q_{glazing}$	Heat gains through windows (W)
$Q_{hb}$	Heat gains through human body (W)
$Q_{l,i}$	Latent heat gains through air infiltration (W)
$Q_{lat}$	Latent heat gains from skin and lungs (W)
$Q_{latent}$	Total latent energy transfer (W)
$Q_m$	Heat gains through fan motor (W)
$Q_{net}$	Total cooling capacity (W)
$Q_{s,i}$	Sensible heat gains through air infiltration (W)
$Q_{sens}$	Sensible heat gains from skin and lungs (W)
$Q_{sensible}$	Total sensible energy transfer (W)
$q_{solar}$	Incident solar radiation ( $W m^{-2}$ )
$Q_{sp}$	Heat gains through floor perimeter (W)
$Q_{wall}$	Heat gains through walls (W)
$Q_{work}$	Heat loss from working human body ( $W m^{-2}$ )
$R_c$	Thermal resistance of clothes ( $m^2 °C W^{-1}$ )
$r_{cb}$	Ratio of clothed to naked body
$T_a$	Ambient air temperature ( $°C$ )
$T_{air}$	Temperature of conditioned air ( $°C$ )
$T_{cloth}$	Temperature of clothes ( $°C$ )
$T_{in}$	Inside air temperature ( $°C$ )
$T_{OA}$	Outside air temperature ( $°C$ )
$T_{out}$	Outside air temperature ( $°C$ )
$T_s$	Surface air temperature ( $°C$ )
$T_{s-a}$	Sol-air temperature ( $°C$ )
$T_{SA}$	Supply air temperature ( $°C$ )

$T_{sur}$	Mean temperature of surrounding surfaces ( $^{\circ}\text{C}$ )
$u$	Volumetric flow of air ( $\text{m}^3 \text{s}^{-1}$ )
$u_{air}$	Velocity of air flow ( $\text{m s}^{-1}$ )
$U_f$	Utilization factor
$U_{floor}$	Overall heat transfer coefficient of floor ( $\text{W m}^{-1} \text{ }^{\circ}\text{C}^{-1}$ )
$U_g$	Overall heat transfer coefficient of glazing ( $\text{W m}^{-1} \text{ }^{\circ}\text{C}^{-1}$ )
$U_{wall}$	Overall heat transfer coefficient ( $\text{W m}^{-1} \text{ }^{\circ}\text{C}^{-1}$ )
$V$	Building volume ( $\text{m}^3$ )
VCAC	Vapor compression air-conditioning system
$W$	Work input (kW)
WBE	Wet-bulb effectiveness
WBT	Wet-bulb temperature
$X_{in}$	Inside air humidity ratio ( $\text{g g}^{-1}$ )
$X_{min}$	Minimum of inlet and outlet air humidity ratios (kg/kg)
$X_{out}$	Outside air humidity ratio ( $\text{g g}^{-1}$ )
$\alpha_{solar}$	Solar absorptivity constant
$\varepsilon_{wb}$	Wet-bulb effectiveness (-)
$\eta_m$	Efficiency of motor
$\rho_{air}$	Density of air ( $\text{kg m}^{-3}$ )
$\varphi$	Solar incident angle relative to the latitude

## References

1. Wang, S.; Tang, R. Supply-based feedback control strategy of air-conditioning systems for direct load control of buildings responding to urgent requests of smart grids. *Appl. Energy* **2017**, *201*, 419–432. [[CrossRef](#)]
2. Mahmood, M.H.; Sultan, M.; Miyazaki, T.; Koyama, S.; Maisotsenko, V.S. Overview of the Maisotsenko cycle—A way towards dew point evaporative cooling. *Renew. Sustain. Energy Rev.* **2016**, *66*, 537–555. [[CrossRef](#)]
3. Sultan, M.; Miyazaki, T.; Saha, B.B.; Koyama, S. Steady-state investigation of water vapor adsorption for thermally driven adsorption based greenhouse air-conditioning system. *Renew. Energy* **2016**, *86*, 785–795. [[CrossRef](#)]
4. Cheng, F.; Li, Y.; Zhang, X.; Li, X. Effect of different absorbents on actual performance of the absorption air-conditioning system based on capacitive deionization regeneration method. *Appl. Therm. Eng.* **2020**, *172*, 115130. [[CrossRef](#)]
5. International Energy Agency (IEA). *Online Data Services*; International Energy Agency (IEA): Paris, France, 2017.
6. Afroz, Z.; Shafiullah, G.M.; Urmee, T.; Higgins, G. Modeling techniques used in building HVAC control systems: A review. *Renew. Sustain. Energy Rev.* **2018**, *83*, 64–84. [[CrossRef](#)]
7. Yang, Z.; Ghahramani, A.; Becerik-Gerber, B. Building occupancy diversity and HVAC (heating, ventilation, and air conditioning) system energy efficiency. *Energy* **2016**, *109*, 641–649. [[CrossRef](#)]
8. Kojok, F.; Fardoun, F.; Younes, R.; Outbib, R. Hybrid cooling systems: A review and an optimized selection scheme. *Renew. Sustain. Energy Rev.* **2016**, *65*, 57–80. [[CrossRef](#)]
9. Duan, Z.; Zhan, C.; Zhang, X.; Mustafa, M.; Zhao, X.; Alimohammadisagvand, B.; Hasan, A. Indirect evaporative cooling: Past, present and future potentials. *Renew. Sustain. Energy Rev.* **2012**, *16*, 6823–6850. [[CrossRef](#)]
10. Duan, Z.; Zhao, X.; Zhan, C.; Dong, X.; Chen, H. Energy saving potential of a counter-flow regenerative evaporative cooler for various climates of China: Experiment-based evaluation. *Energy Build.* **2017**, *148*, 199–210. [[CrossRef](#)]
11. Liu, Y.; Yang, X.; Li, J.; Zhao, X. Energy savings of hybrid dew-point evaporative cooler and micro-channel separated heat pipe cooling systems for computer data centers. *Energy* **2018**, *163*, 629–640. [[CrossRef](#)]
12. Matsui, K.; Thu, K.; Miyazaki, T. A Hybrid Power Cycle using an Inverted Brayton Cycle with an Indirect Evaporative Device for Waste-heat Recovery. *Appl. Therm. Eng.* **2020**, 115029. [[CrossRef](#)]
13. Farmahini-Farahani, M.; Delfani, S.; Esmaelian, J. Exergy analysis of evaporative cooling to select the optimum system in diverse climates. *Energy* **2012**, *40*, 250–257. [[CrossRef](#)]

14. Lin, J.; Bui, D.T.; Wang, R.; Chua, K.J. On the exergy analysis of the counter-flow dew point evaporative cooler. *Energy* **2018**, *165*, 958–971. [[CrossRef](#)]
15. Alklaibi, A.M. Experimental and theoretical investigation of internal two-stage evaporative cooler. *Energy Convers. Manag.* **2015**, *95*, 140–148. [[CrossRef](#)]
16. Fikri, B.; Sofia, E.; Putra, N. Experimental analysis of a multistage direct-indirect evaporative cooler using a straight heat pipe. *Appl. Therm. Eng.* **2020**, *171*, 115133. [[CrossRef](#)]
17. Khalajzadeh, V.; Farmahini-Farahani, M.; Heidarinejad, G. A novel integrated system of ground heat exchanger and indirect evaporative cooler. *Energy Build.* **2012**, *49*, 604–610. [[CrossRef](#)]
18. Chauhan, S.S.; Rajput, S.P.S. Experimental analysis of an evaporative–vapour compression based combined air conditioning system for required comfort conditions. *Appl. Therm. Eng.* **2017**, *115*, 326–336. [[CrossRef](#)]
19. Duan, Z.; Zhao, X.; Liu, J.; Zhang, Q. Dynamic simulation of a hybrid dew point evaporative cooler and vapour compression refrigerated system for a building using EnergyPlus. *J. Build. Eng.* **2019**, *21*, 287–301. [[CrossRef](#)]
20. Zhou, S.; Gong, L.; Liu, X.; Shen, S. Mathematical modeling and performance analysis for multi-effect evaporation/multi-effect evaporation with thermal vapor compression desalination system. *Appl. Therm. Eng.* **2019**, *159*, 113759. [[CrossRef](#)]
21. Rostamzadeh, H.; Rostamzadeh, J.; Matin, P.S.; Ghaebi, H. Novel dual-loop bi-evaporator vapor compression refrigeration cycles for freezing and air-conditioning applications. *Appl. Therm. Eng.* **2018**, *138*, 563–582. [[CrossRef](#)]
22. Hong, H.; Li, W.; Gu, C. Performance study on a mechanical vapor compression evaporation system driven by Roots compressor. *Int. J. Heat Mass Transf.* **2018**, *125*, 343–349. [[CrossRef](#)]
23. Kim, M.-H.; Jeong, J.-W. Cooling performance of a 100% outdoor air system integrated with indirect and direct evaporative coolers. *Energy* **2013**, *52*, 245–257. [[CrossRef](#)]
24. Hasan, A. Indirect evaporative cooling of air to a sub-wet bulb temperature. *Appl. Therm. Eng.* **2010**, *30*, 2460–2468. [[CrossRef](#)]
25. Delfani, S.; Esmaeliani, J.; Pasdarsahri, H.; Karami, M. Energy saving potential of an indirect evaporative cooler as a pre-cooling unit for mechanical cooling systems in Iran. *Energy Build.* **2010**, *42*, 2169–2176. [[CrossRef](#)]
26. Heidarinejad, G.; Bozorgmehr, M.; Delfani, S.; Esmaeliani, J. Experimental investigation of two-stage indirect/direct evaporative cooling system in various climatic conditions. *Build. Environ.* **2009**, *44*, 2073–2079. [[CrossRef](#)]
27. Chiesa, G.; Huberman, N.; Pearlmutter, D. Geo-climatic potential of direct evaporative cooling in the Mediterranean Region: A comparison of key performance indicators. *Build. Environ.* **2019**, *151*, 318–337. [[CrossRef](#)]
28. Sohani, A.; Sayyaadi, H. Thermal comfort based resources consumption and economic analysis of a two-stage direct-indirect evaporative cooler with diverse water to electricity tariff conditions. *Energy Convers. Manag.* **2018**, *172*, 248–264. [[CrossRef](#)]
29. Jaber, S.; Ezzat, A.W. Investigation of energy recovery with exhaust air evaporative cooling in ventilation system. *Energy Build.* **2017**, *139*, 439–448. [[CrossRef](#)]
30. Aparicio-Ruiz, P.; Schiano-Phan, R.; Salmerón-Lissén, J.M. Climatic applicability of downdraught evaporative cooling in the United States of America. *Build. Environ.* **2018**, *136*, 162–176. [[CrossRef](#)]
31. Sultan, M.; El-Sharkawy, I.I.; Miyazaki, T.; Saha, B.B.; Koyama, S.; Maruyama, T.; Maeda, S.; Nakamura, T. Water vapor sorption kinetics of polymer based sorbents: Theory and experiments. *Appl. Therm. Eng.* **2016**, *106*, 192–202. [[CrossRef](#)]
32. Hanif, S.; Sultan, M.; Miyazaki, T. Effect of relative humidity on thermal conductivity of zeolite-based adsorbents: Theory and experiments. *Appl. Therm. Eng.* **2019**, *150*, 11–18. [[CrossRef](#)]
33. Shabir, F.; Sultan, M.; Miyazaki, T.; Saha, B.B.; Askalany, A.; Ali, I.; Zhou, Y.; Ahmad, R.; Shamshiri, R.R. Recent updates on the adsorption capacities of adsorbent-adsorbate pairs for heat transformation applications. *Renew. Sustain. Energy Rev.* **2020**, *119*, 109630. [[CrossRef](#)]
34. Kim, M.-H.; Yoon, D.-S.; Kim, H.-J.; Jeong, J.-W. Retrofit of a liquid desiccant and evaporative cooling-assisted 100% outdoor air system for enhancing energy saving potential. *Appl. Therm. Eng.* **2016**, *96*, 441–453. [[CrossRef](#)]

35. Ham, S.-W.; Lee, S.-J.; Jeong, J.-W. Operating energy savings in a liquid desiccant and dew point evaporative cooling-assisted 100% outdoor air system. *Energy Build.* **2016**, *116*, 535–552. [[CrossRef](#)]
36. Cuce, P.M. Thermal performance assessment of a novel liquid desiccant-based evaporative cooling system: An experimental investigation. *Energy Build.* **2017**, *138*, 88–95. [[CrossRef](#)]
37. Cho, H.-J.; Jeong, J.-W. Evaluation of thermal comfort in an office building served by a liquid desiccant-assisted evaporative cooling air-conditioning system. *Energy Build.* **2018**, *172*, 361–370. [[CrossRef](#)]
38. Kashif Shahzad, M.; Qadar Chaudhary, G.; Ali, M.; Ahmed Sheikh, N.; Shahid Khalil, M.; Rashid, T.U. Experimental evaluation of a solid desiccant system integrated with cross flow Maisotsenko cycle evaporative cooler. *Appl. Therm. Eng.* **2018**, *128*, 1476–1487. [[CrossRef](#)]
39. Sultan, M.; El-Sharkawy, I.I.; Miyazaki, T.; Saha, B.B.; Koyama, S. An overview of solid desiccant dehumidification and air conditioning systems. *Renew. Sustain. Energy Rev.* **2015**, *46*, 16–29. [[CrossRef](#)]
40. Sultan, M.; Mahmood, M.H.; Miyazaki, T.; Koyama, S.; Khan, Z.M. Close and open cycle adsorption kinetics: Development of correlation for desiccant air-conditioning. *J. Eng. Appl. Sci.* **2016**, *35*, 59–66.
41. Mahmood, M.H.; Sultan, M.; Miyazaki, T. Experimental evaluation of desiccant dehumidification and air-conditioning system for energy-efficient storage of dried fruits. *Build. Serv. Eng. Res. Technol.* **2019**, 0143624419893660. [[CrossRef](#)]
42. Sultan, M.; Miyazaki, T.; Mahmood, M.; Mahmood Khan, Z. Solar assisted evaporative cooling based passive air-conditioning system for agricultural and livestock applications. *J. Eng. Sci. Technol.* **2018**, *13*, 693–703.
43. Sultan, M.; Miyazaki, T. Energy-efficient air-conditioning systems for nonhuman applications. In *Refrigeration*; Ekren, O., Ed.; InTech: London, UK, 2017.
44. Sultan, M.; Miyazaki, T.; Koyama, S. Optimization of adsorption isotherm types for desiccant air-conditioning applications. *Renew. Energy* **2018**, *121*, 441–450. [[CrossRef](#)]
45. Sultan, M.; Miyazaki, T.; Koyama, S.; Khan, Z.M. Performance evaluation of hydrophilic organic polymer sorbents for desiccant air-conditioning applications. *Adsorpt. Sci. Technol.* **2018**, *36*, 311–326. [[CrossRef](#)]
46. Kashif, M.; Niaz, H.; Sultan, M.; Miyazaki, T.; Feng, Y.; Usman, M.; Shahzad, M.W.; Niaz, Y.; Waqas, M.M.; Ali, I. Study on Desiccant and Evaporative Cooling Systems for Livestock Thermal Comfort: Theory and Experiments. *Energies* **2020**, *13*, 2675. [[CrossRef](#)]
47. Kottek, M.; Grieser, J.; Beck, C.; Rudolf, B.; Rubel, F. World map of the Köppen-Geiger climate classification updated. *Meteorol. Z.* **2006**, *15*, 259–263. [[CrossRef](#)]
48. Niaz, H.; Sultan, M.; Khan, A.; Mahmood, M.; Feng, Y.; Mahmood Khan, Z.; Niaz, E.D.Y.; Ali, I.; Imran, M. Study on evaporative cooling assisted desiccant air-conditioning system for livestock application in Pakistan. *Fresenius Environ. Bull.* **2019**, *28*, 8623–8633.
49. Chen, J.; Ding, R.; Li, Y.; Lin, X.; Chen, Y.; Luo, X.; Yang, Z. Application of a vapor–liquid separation heat exchanger to the air conditioning system at cooling and heating modes. *Int. J. Refrig.* **2019**, *100*, 27–36. [[CrossRef](#)]
50. *ASHRAE Handbook of Fundamentals*. Am. Soc. Heating, Refrig; Air-Conditioning Eng. Inc.: Atlanta, GA, USA, 2013.
51. Havenith, G.; Kuklane, K.; Fan, J.; Hodder, S.; Ouzzahra, Y.; Lundgren, K.; Au, Y.; Loveday, D. A database of static clothing thermal insulation and vapor permeability values of non-Western ensembles for use in ASHRAE standard 55, ISO 7730, and ISO 9920. *ASHRAE Trans.* **2015**, *121*, 197–215.
52. Designbuilder Software Limited. *DesignBuilder 6.1*; Designbuilder Software Limited: Stroud, UK, 2020.
53. U.S. Department of Energy (DOE); National Renewable Energy Laboratory (NREL). *EnergyPlus 9.3*; U.S. Department of Energy (DOE): Washington, DC, USA; National Renewable Energy Laboratory (NREL): Golden, CO, USA, 2020.
54. Shen, B.; New, J.; Baxter, V. Air source integrated heat pump simulation model for EnergyPlus. *Energy Build.* **2017**, *156*, 197–206. [[CrossRef](#)]
55. Kang, W.H.; Lee, J.M.; Yeon, S.H.; Park, M.K.; Kim, C.H.; Lee, J.H.; Moon, J.W.; Lee, K.H. Modeling, calibration, and sensitivity analysis of direct expansion AHU-Water source VRF system. *Energy* **2020**, *199*, 117435. [[CrossRef](#)]
56. Seo, B.; Yoon, Y.B.; Yu, B.H.; Cho, S.; Lee, K.H. Comparative analysis of cooling energy performance between water-cooled VRF and conventional AHU systems in a commercial building. *Appl. Therm. Eng.* **2020**, *170*, 114992. [[CrossRef](#)]

57. Naderi, E.; Sajadi, B.; Behabadi, M.A.; Naderi, E. Multi-objective simulation-based optimization of controlled blind specifications to reduce energy consumption, and thermal and visual discomfort: Case studies in Iran. *Build. Environ.* **2020**, *169*, 106570. [[CrossRef](#)]
58. Im, P.; Joe, J.; Bae, Y.; New, J.R. Empirical validation of building energy modeling for multi-zones commercial buildings in cooling season. *Appl. Energy* **2020**, *261*, 114374. [[CrossRef](#)]
59. Salata, F.; Ciancio, V.; Dell’Olmo, J.; Golasi, I.; Palusci, O.; Coppi, M. Effects of local conditions on the multi-variable and multi-objective energy optimization of residential buildings using genetic algorithms. *Appl. Energy* **2020**, *260*, 114289. [[CrossRef](#)]
60. Rosso, F.; Ciancio, V.; Dell’Olmo, J.; Salata, F. Multi-objective optimization of building retrofit in the Mediterranean climate by means of genetic algorithm application. *Energy Build.* **2020**, *216*, 109945. [[CrossRef](#)]
61. Wang, H.; Lu, W.; Wu, Z.; Zhang, G. Parametric analysis of applying PCM wallboards for energy saving in high-rise lightweight buildings in Shanghai. *Renew. Energy* **2020**, *145*, 52–64. [[CrossRef](#)]
62. Qiu, C.; Yi, Y.K.; Wang, M.; Yang, H. Coupling an artificial neuron network daylighting model and building energy simulation for vacuum photovoltaic glazing. *Appl. Energy* **2020**, *263*, 114624. [[CrossRef](#)]
63. Ascione, F.; Bianco, N.; Iovane, T.; Mauro, G.M.; Napolitano, D.F.; Ruggiano, A.; Viscido, L. A real industrial building: Modeling, calibration and Pareto optimization of energy retrofit. *J. Build. Eng.* **2020**, *29*, 101186. [[CrossRef](#)]
64. Troup, L.N.; Fannon, D.J.; Eckelman, M.J. Spatio-temporal changes among site-to-source conversion factors for building energy modeling. *Energy Build.* **2020**, *213*, 109832. [[CrossRef](#)]
65. Martin, M.; Wong, N.H.; Hii, D.J.C.; Ignatius, M. Comparison between simplified and detailed EnergyPlus models coupled with an urban canopy model. *Energy Build.* **2017**, *157*, 116–125. [[CrossRef](#)]
66. Qin, H.; Pan, W. Energy use of subtropical high-rise public residential buildings and impacts of energy saving measures. *J. Clean. Prod.* **2020**, *254*, 120041. [[CrossRef](#)]
67. Crawley, D.B.; Hand, J.W.; Kummert, M.; Griffith, B.T. Contrasting the capabilities of building energy performance simulation programs. *Build. Environ.* **2008**, *43*, 661–673. [[CrossRef](#)]
68. Bojić, M.; Nikolić, N.; Nikolić, D.; Skerlić, J.; Miletić, I. Toward a positive-net-energy residential building in Serbian conditions. *Appl. Energy* **2011**, *88*, 2407–2419. [[CrossRef](#)]
69. Woods, J.; Bonnema, E. Regression-based approach to modeling emerging HVAC technologies in EnergyPlus: A case study using a Vuilleumier-cycle heat pump. *Energy Build.* **2019**, *186*, 195–207. [[CrossRef](#)]
70. Anđelković, A.S.; Mujan, I.; Dakić, S. Experimental validation of a EnergyPlus model: Application of a multi-storey naturally ventilated double skin façade. *Energy Build.* **2016**, *118*, 27–36. [[CrossRef](#)]
71. Cho, H.M.; Wi, S.; Chang, S.J.; Kim, S. Hygrothermal properties analysis of cross-laminated timber wall with internal and external insulation systems. *J. Clean. Prod.* **2019**, *231*, 1353–1363. [[CrossRef](#)]
72. Karimi, M.S.; Fazelpour, F.; Rosen, M.A.; Shams, M. Comparative study of solar-powered underfloor heating system performance in distinctive climates. *Renew. Energy* **2019**, *130*, 524–535. [[CrossRef](#)]
73. Ceballos-Fuentealba, I.; Álvarez-Miranda, E.; Torres-Fuchslocher, C.; del Campo-Hitschfeld, M.L.; Díaz-Guerrero, J. A simulation and optimisation methodology for choosing energy efficiency measures in non-residential buildings. *Appl. Energy* **2019**, *256*, 113953. [[CrossRef](#)]
74. Zhang, A.; Bokel, R.; van den Dobbelsteen, A.; Sun, Y.; Huang, Q.; Zhang, Q. An integrated school and schoolyard design method for summer thermal comfort and energy efficiency in Northern China. *Build. Environ.* **2017**, *124*, 369–387. [[CrossRef](#)]
75. Abdeen, A.; Serageldin, A.A.; Ibrahim, M.G.E.; El-Zafarany, A.; Ookawara, S.; Murata, R. Experimental, analytical, and numerical investigation into the feasibility of integrating a passive Trombe wall into a single room. *Appl. Therm. Eng.* **2019**, *154*, 751–768. [[CrossRef](#)]
76. Venkateswara Rao, V.; Datta, S.P. A feasibility assessment of single to multi/hybrid evaporative coolers for building air-conditioning across diverse climates in India. *Appl. Therm. Eng.* **2020**, *168*, 114813. [[CrossRef](#)]
77. Thermal Energy System Specialists LLC. *TRNSYS 17*; Thermal Energy System Specialists LLC: Madison, WI, USA, 2019.
78. ASHRAE Standards Committee. *ANSI/ASHRAE Standard 143-2007, Method of Test for Rating Indirect Evaporative Coolers*; ASHRAE Standards Committee: Atlanta, GA, USA, 2007.
79. DuBois, D.F. A formula to estimate the approximate surface area if height and body mass be known. *Arch. Intern. Med.* **1916**, *17*, 863–871. [[CrossRef](#)]

80. Cengel, Y. *Heat and Mass Transfer: Fundamentals and Applications*; McGraw-Hill Higher Education: New York, NY, USA, 2014; ISBN 0077654765.
81. Kreider, J.F.; Curtiss, P.S.; Rabl, A. *Heating and Cooling of Buildings: Design for Efficiency*; CRC Press: Boca Raton, FL, USA, 2009; ISBN 1439882509.
82. ISO. *ISO 7730, Ergonomics of the Thermal Environment—Analytical Determination and Interpretation of Thermal Comfort Using Calculation of the PMV and PPD Indices and Local Thermal Comfort Criteria*; ISO: Geneva, Switzerland, 2005.
83. Raza, H.M.U. Investigation of Evaporative Cooling Based Low-Cost Air-Conditioning Technologies for Pakistan. Master's Thesis (Hons.), Bahauddin Zakariya University, Multan, Pakistan, 2018.
84. Teitelbaum, E.; Jayathissa, P.; Miller, C.; Meggers, F. Design with Comfort: Expanding the psychrometric chart with radiation and convection dimensions. *Energy Build.* **2020**, *209*, 109591. [[CrossRef](#)]
85. Yousuf, I.; Ghumman, A.R.; Hashmi, H.N.; Kamal, M.A. Carbon emissions from power sector in Pakistan and opportunities to mitigate those. *Renew. Sustain. Energy Rev.* **2014**, *34*, 71–77. [[CrossRef](#)]



© 2020 by the authors. Licensee MDPI, Basel, Switzerland. This article is an open access article distributed under the terms and conditions of the Creative Commons Attribution (CC BY) license (<http://creativecommons.org/licenses/by/4.0/>).